Computer Assisted Mechanics and Engineering Sciences, 5: 267–283, 1998.


# The space–time approach to rail/wheel contact and corrugations problem

Czesław I. Bajer
*Institute of Fundamental Technological Research, Polish Academy of Sciences, Świętokrzyska 21, 00-049 Warsaw, Poland*

(Received May 19, 1997)

The paper presents a space–time discrete modeling of the dynamic rail-wheel contact problem and an analysis of the induced corrugations. First, the space–time approach to simple contact problems is presented. Then, the resulting differential equation of motion is solved by discrete time integration. An arbitrary mesh modification, both in time and space, enables an easy modeling of rapidly varying contact zone. The velocity formulation is used and the discontinuity of the velocity in the contact is removed by a special algorithm. Finally the discussed technique is used to simulate interaction of the elastic wheel and rigid rail. It is shown that the contact force oscillates and the material of the wheel rotates oscillatory.

## 1. INTRODUCTION

The problem of corrugations (waved surface) in railway industry or metal rolling in steel rails has been undertaken in several research and technological centers in the world. Different hypotheses were assumed as a starting point of investigation. Some of them can easily be rejected, others require intensive theoretical and experimental tests. In the relevant literature the following cases are considered as a source of corrugations of both the wheel and rail surface:

- imperfections in rail joints,
- cone form of wheels which results in different linear speed of left and right wheel (causing snaking of trains and, in general, disturbed steady motion),
- periodical structure of rails (sleepers); instability of motion on the periodically placed supports,
- contact between wheel and rail; stick and slip sections which vary with high frequency (horizontally) generate waves which result in elastic-plastic response of the metal surfaces,
- residual deformations in the stage of manufacturing of rails,
- nonlinear and strongly time-dependent friction law in the contact zone,
- influence of material hardening,
- deformation of elements of wheel/axis in the vehicle system.

An actual picture of a corrugated surface of the wheel and rail is presented in Fig. 1. The corrugation problem is of primary importance in both the railways (wear [1] and noise [2]) and steel industries (sheet rolling). Existing hypotheses [3, 4] do not include important conditions in which corrugations occur. Numerical simulations of the rolling contact problem with the use of F.E.M. were limited to the quasi-static analysis of rolling of the elastic-plastic band [5, 6, 7] or short term simulation of non-stationary process [8]. Typically the F.E.M. was used to determine the eigenfrequencies of subsystems [3, 9, 10] and for a search of relations between the wave length of corrugations and relative speed of motion.

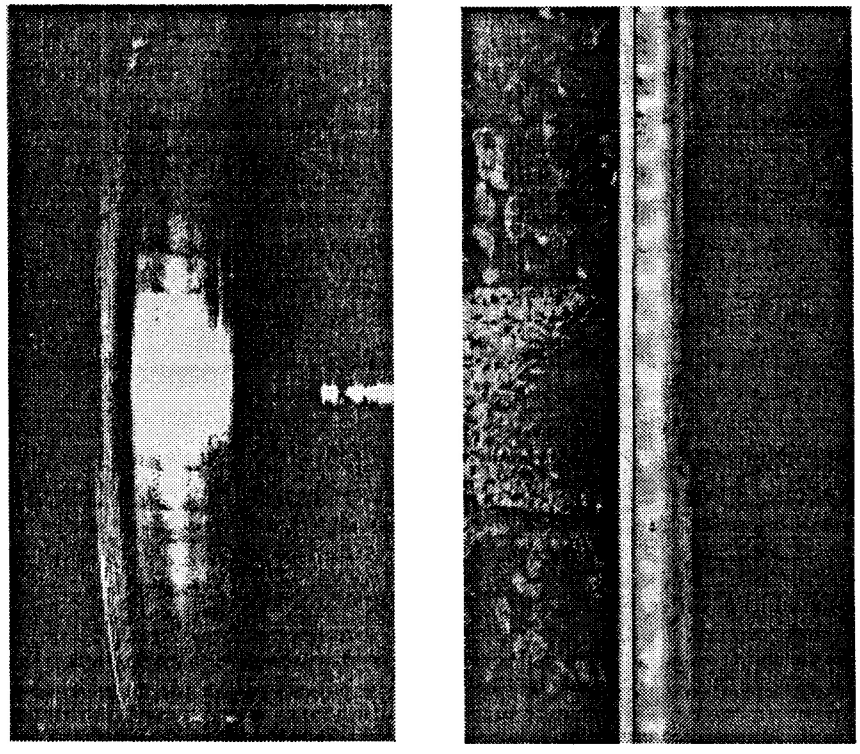

**Fig. 1.** Corrugations of wheel and rail

The thorough examination of the problem requires taking into account the theory of plasticity, theory of vibration, friction and wear. Due to complexity of the vehicle or rolling machine, the analytic approach to the problem is extremely difficult. This paper is not intended to discuss this wide and complex problem. Mutual co-existence of several reasons which occur in the same time with different intensity makes the problem difficult even in a particular case. In the following sections we shall rather try to answer one of questions: how the waved or corrugated surface can be created in the case of an almost steady motion.

The aim of the paper is to develop the way of tackling the problem of evolution of solid systems and the geometrical constraints of motion. The limitations are imposed by the history of the velocity field. Several possibilities for accounting for the unilateral contact are available. However, numerical experiments show that the computational time depends strongly on the choice of the solution method of the given problem. The choice of geometrical constraints constitutes restrictions imposed on the variation of the velocity field and allows us to gain a substantial reduction of the computational time.

The present paper is organized as follows.

First, a formulation is presented, which is particularly suitable for many different problems, such as rigid mechanisms or deformable solid system subjected to dynamical loading. It should be noted that the choice of the velocity formulation is not incompatible with the description of the deformation or displacement field. Moreover, the resulting expressions are less intricate and the contact evolution between deformable solids is more simple since it is a tangent space formulation.

The basic general formulation of the problem (instantaneous updated Lagrangian formulation) is well adapted for the discretization by the Space–Time Finite Element Method, which avoids the dissociation of the space discretization and time discretization. The virtual work principle is formulated by integrating with respect to time the virtual power principle. The velocity field is assumed to be the main variable. The proposed space–time elements have a linear dependence of the parameters in time. The choice of virtual velocity field is discussed in great details.

The problem of contacting points can be formulated by the introduction of special elements. These elements have extra time nodal points that are eliminated by the typical contact conditions. The interpolation functions are piece-wise time dependent.

The tangential conditions are formulated via the reological type friction law. Tensor theory allows to connect the space and surface behavior. Some conditions of compatibility have to be fulfilled but a phenomenological way is open to choose the more suitable law to special problem with dry or lubricated friction. The viscoplastic friction law is more real when applied to the forming problems.

The solution algorithm uses a fixed point Newton–Raphson method which allows to save the computational time. The algorithm uses a frontal method that leads to the solution of a problem of the same size as the classical finite element method. Therefore the classical software can simply be adapted to implement the results presented in this paper.

## 2. THE SPACE–TIME VELOCITY APPROACH FORMULATION

The approach used in the present work was already described in several papers [11, 12, 13, 14, 15, 16, 17, 18, 19, 20, 21]. In the following we shall only present a short introduction to the problem.

In the case of a linear interpolation for displacements the domain at $t$ can be simply described by the formula (the Minkowski transformation) (Fig. 2):

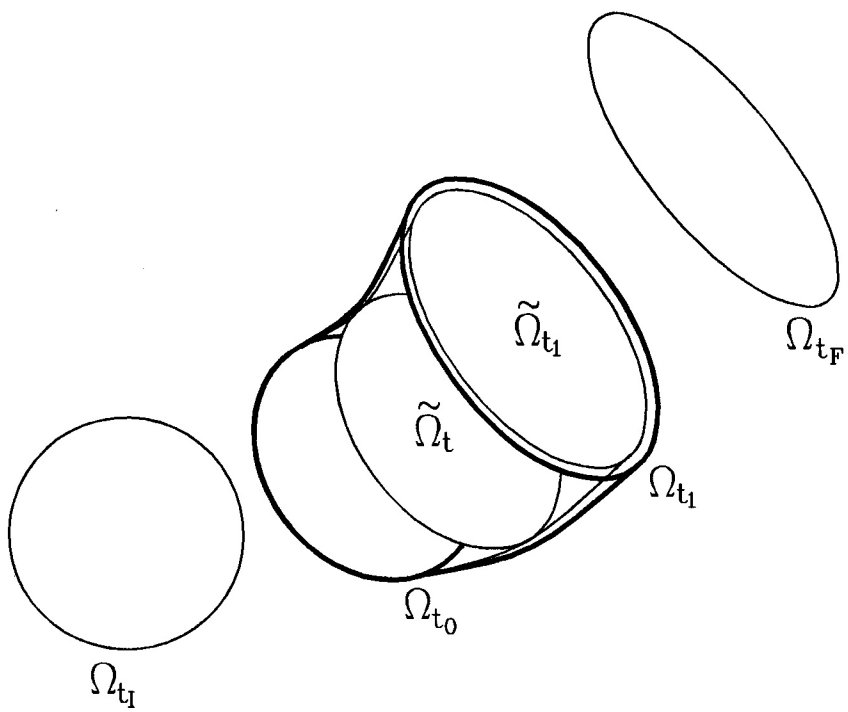


**Fig. 2.** Description of the evolution of the domain deformation

$$\Omega_t = \Omega_{t_0}\left(1 - \frac{t - t_0}{h}\right) + \Omega_{t_1}\frac{t - t_0}{h}, \quad h = t_1 - t_0 \ , \tag{1}$$

where $\Omega_t$ is an intermediate geometry in time $t$, while $\Omega_{t_0}$ and $\Omega_{t_1}$ are geometries in time $t_0$ and $t_1$, respectively.

For a linear interpolation of the velocity $\Omega_t$ depends on $x_0$, $v_0$, $v_1$:

$$\mathbf{x} = \mathbf{x}_0 + \mathbf{v}_0\frac{1}{2}(2 - \tau)h + \mathbf{v}_1\frac{\tau}{2}h \tag{2}$$

where:
$\tau = \frac{t-t_0}{h}$, $\Omega_{t_0} = \{\mathbf{x}_0\}$, $\Omega_{t_1} = \{\mathbf{x}_0\} + \left\{\frac{\mathbf{v}_0+\mathbf{v}_1}{2}h\right\}$. The solution to the velocity field will be postulated as a product of a space and a time functions.

On this short background we can develop a space–time approximation. Essentially, the basic principle of the method is concerned with the way of approximation. Characteristic functions (i.e. displacements, velocities) are described in space–time subdomains by nodal parameters

$$\mathbf{u}(\mathbf{x},t) = \mathbf{N}(\mathbf{x},t)\,\mathbf{q}_e \tag{3}$$

where $\mathbf{N}(\mathbf{x},t)$ is the matrix of interpolation functions, which depends on spatial and time variables. Such an approach assumes the continuous distribution of characteristic quantities in the whole space–time domain $\Omega$, in which the structure is considered, $\Omega = \{\mathbf{x},t : \mathbf{x} \in V(t), 0 \leq t < \infty\}$. In discrete time $t_i$, $i$=1, 2,..., we can use different bases of nodes (limited by certain restrictions) and according to this feature we can adjust the mesh to our current requirements. This approach has the following advantages:

- mesh redistribution according to the error distribution, which varies in time,
- relocation of the condensed mesh together with the moving load,
- use of different forms of meshes (different from the multiplex type, which is a result of evolution of the spatial mesh in the time layer); some meshes have certain interesting properties [11],
- simple individual formulation of properties of time integration, separately for each finite element,
- in a particular case the space–time approximation can be reduced to the classical solution method, based on the evolution of the material mesh.

The last point can be also expressed in the form: the space–time approximation and the method of the space–time finite elements can be considered as a generalization of the finite element method (which in fact is directly applied only to spatial domain).

### 2.1. Basics of the space–time finite element method

We shall start from the differential equation of motion

$$m\frac{\mathrm{d}v}{\mathrm{d}t} + kx = 0\,. \tag{4}$$

The principle of virtual power gives an alternative formulation

$$\left(m\frac{\mathrm{d}v}{\mathrm{d}t} + kx\right)v^* = 0\,, \tag{5}$$

where $v^*$ is a virtual velocity function.

We shall further assume a linear velocity distribution $v$ over the time interval $0 \leq t \leq h$.

$$v = \left(1-\frac{t}{h}\right)v_0 + \frac{t}{h}v_1\,. \tag{6}$$

Thus the displacement $x(t)$ is described by the integral

$$x(t) = \int_0^t v\,\mathrm{d}t = h_0 + \frac{h}{2}\left[1-\left(1-\frac{t}{h}\right)^2\right]v_0 + \frac{t^2}{2h}v_1\,. \tag{7}$$

In the following the proper choice of distribution of the virtual velocity $v^*$ is the fundamental problem of the method. The convergence, efficiency, accuracy of time integration and accuracy of

the solution in the case of geometrical nonlinearities depend on the form of $v^*$. The simplest choice is the Dirac distribution:

$$v^* = v_1 \, \delta\left(\frac{t}{h} - \alpha\right), \qquad 0 \leq \alpha \leq 1. \tag{8}$$

The distribution (8) is convenient for our purpose since it reduces the computational effort and allows us to select the parameter $\alpha$ according to the stability condition.

Substituting Eqs.(6), (7) and (8) into Eq.(5) and integrating with respect to time in the time interval $[0, h]$ gives:

$$v_1 = \frac{1 - \frac{kh^2}{2m}[1 - (1-\alpha)^2]}{1 + \frac{k\alpha^2 h^2}{2m}} v_0 - \frac{k}{m} \frac{h}{\left(1 + \frac{k\alpha^2 h^2}{2m}\right)} x_0 \, . \tag{9}$$

This formula allows us to compute $v_1$ provided the initial conditions $v_0$, $x_0$ for the time step $[0, h]$ are known. Now, the geometry $x_1$ is the last unknown which must be determined before proceeding to the next step $[h, 2h]$. The average value of the velocity taken at point $\beta h$, $0 \leq \beta \leq 1$ results in the formula

$$x_1 = x_0 + h[(1-\beta)v_0 + \beta v_1] \, . \tag{10}$$

The energy at the end of the time interval is preserved if $\beta = 1 - \alpha$ . Then we have finally

$$x_1 = x_0 + h[\alpha v_0 + (1-\alpha)v_1] \, . \tag{11}$$

It was proved in [22] that the unconditional stability of the process (9), (11) occurs for $\frac{\sqrt{2}}{2} \leq \alpha \leq 1$. For $\alpha$=1 we have the explicit formula while for other values ($0 \leq \alpha < 1$) the scheme is implicit and requires iterations to determine the geometry $x_1$.

### 2.2. The space–time finite element formulation

We consider the variation of the multidimensional geometry in time (Fig. 3). The space–time volume is bounded by the initial and final domain.

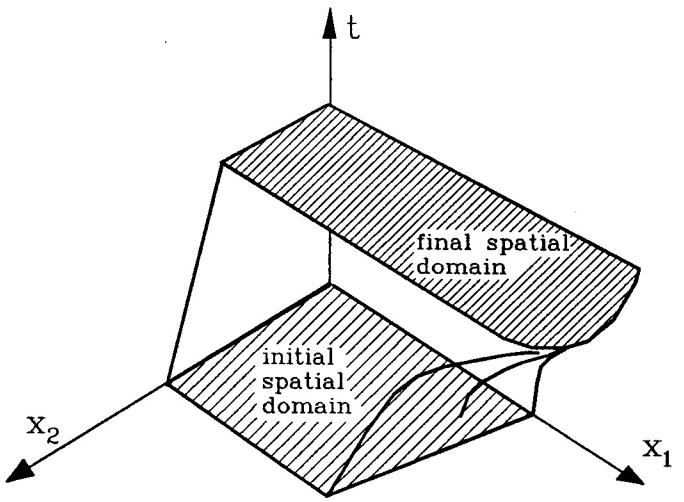


**Fig. 3.** Evolution of the spatial domain in two dimensions

Let us now consider a more general approach to multi-dimensional cases. If the strain measure $\boldsymbol{\varepsilon}$ is defined as

$$\boldsymbol{\varepsilon} = \mathcal{D}\mathbf{u} \,, \tag{12}$$

where $\mathcal{D}$ is the differential operator, and $\boldsymbol{\sigma}$ is the II Piola–Kirchhoff the stress tensor

$$\boldsymbol{\sigma} = \mathbf{E}\boldsymbol{\varepsilon} \,, \tag{13}$$

then assuming the distribution of virtual velocities $\mathbf{v}^*$, the equation of virtual work described by velocity assumes the following form:

$$\int_\Omega (\mathbf{v}^*)^T \rho \frac{\partial \mathbf{v}}{\partial t} \mathrm{d}\Omega + \int_\Omega (\dot{\boldsymbol{\varepsilon}}^*)^T \boldsymbol{\sigma} \mathrm{d}\Omega + \int_\Omega (\mathbf{v}^*)^T \eta_z \mathbf{v} \, \mathrm{d}\Omega = 0 \,. \tag{14}$$

where $\rho$ is the mass density and $\eta_z$ is the external damping coefficient.

The displacement $\mathbf{u}(t)$ is defined as the integral (see Eq. 7)

$$\mathbf{u}(t) = \mathbf{u}_0 + \int_0^t \mathbf{v} \, \mathrm{d}t \,. \tag{15}$$

Combining Eqs. (12), (13) and (15) we get:

$$\int_\Omega (\mathbf{v}^*)^T \rho \frac{\partial \mathbf{v}}{\partial t} \mathrm{d}\Omega + \int_\Omega (\mathcal{D}\mathbf{v}^*)^T \mathbf{E} \mathcal{D}\mathbf{u}_0 \mathrm{d}\Omega + \int_\Omega \left[ (\mathcal{D}\mathbf{v}^*)^T \, \mathbf{E} \, \mathcal{D} \int_0^t \mathbf{v} \, \mathrm{d}t \right] \mathrm{d}\Omega + \int_\Omega (\mathbf{v}^*)^T \eta_z \mathbf{v} \, \mathrm{d}\Omega = 0 \,. \tag{16}$$

In the next step we define the interpolation functions:

$$\mathbf{v} = \mathbf{N}\dot{\mathbf{q}} \quad \text{and} \quad \mathbf{v}^* = \mathbf{N}^*\dot{\mathbf{q}} \,, \tag{17}$$

which finally gives:

$$\left\{ \int_\Omega \left[ (\mathcal{D}\mathbf{N}^*)^T \, \mathbf{E} \, \mathcal{D} \int_0^t \mathbf{N} \, \mathrm{d}t \right] \mathrm{d}\Omega + \int_\Omega (\mathbf{N}^*)^T \rho \frac{\partial \mathbf{N}}{\partial t} \mathrm{d}\Omega + \int_\Omega (\mathbf{N}^*)^T \eta_z \, \mathbf{N} \, \mathrm{d}\Omega \right\} \dot{\mathbf{q}} + \int_\Omega (\mathcal{D}\mathbf{N}^*)^T \, \mathbf{E} \, \boldsymbol{\varepsilon}_0 \, \mathrm{d}\Omega = \mathbf{0} \,, \tag{18}$$

or in a short form

$$(\mathbf{K} + \mathbf{M} + \mathbf{Z})\mathbf{v} + \mathbf{s} = \mathbf{0} \,. \tag{19}$$

Assuming further that the distribution of the virtual displacements, which depends on the nodal parameters only, is determined in time $t = h$, we can obtain in (18) upper halfs of the matrices $\mathbf{M}$, $\mathbf{K}$ and the vector $\mathbf{s}$ equal to zero. As in the case of one degree of freedom system we can change the value of parameter $\alpha$ and in this way we can modify the property of the procedure.

At this point we can briefly discuss the computational costs of the proposed procedure. First let us step back to the assumption on the virtual distribution of the nodal parameters. The Dirac distribution in time reduces the problem of the integration in the space–time volume $\Omega$ to the integration over the surface $t = \alpha h$, with respect to spatial variables $x, y, z$ only. It decreases the computational cost as compared to classical, linear interpolation of the virtual nodal parameters in time.

In the case of Eq. (18) the domain of integration is reduced from the space-time volume $\Omega$ to the surface (real volume) $V(\alpha h)$. The first integral contains the term integrated in $[0,t]$. Practically, it is sufficient to integrate in $[0,\alpha h]$. If linear real functions $\mathbf{N}$ are assumed we can compute the mean value of the integrated term for $t=\alpha h/2$ and multiply it by the length of the time interval. Then the stiffness and mass matrices and initial stress vector in the element are as follows:

$$\mathbf{K}=\int\int_{V_{\alpha h}} (\mathcal{D}\mathbf{N}_{\alpha h}(\mathbf{x}))^T\,\mathbf{E}\,\mathcal{D}\mathbf{N}(\mathbf{x},\alpha h/2)\,\mathrm{d}V\cdot\alpha h\,, \tag{20}$$

$$\mathbf{M}=\int\int_{V_{\alpha h}} \mathbf{N}_{\alpha h}^T(\mathbf{x})\,\rho\,\frac{\partial\mathbf{N}(\mathbf{x},\alpha h)}{\partial t}\,\mathrm{d}V\,, \tag{21}$$

$$\mathbf{Z}=\int\int_{V_{\alpha h}} \mathbf{N}_{\alpha h}^T(\mathbf{x})\,\eta_z\,\mathbf{N}(\mathbf{x},\alpha h)\,\mathrm{d}V\,, \tag{22}$$

$$\mathbf{s}=\int\int_{V_{\alpha h}} (\mathcal{D}\mathbf{N}_{\alpha h}(\mathbf{x}))^T\,\mathbf{E}\,\boldsymbol{\varepsilon}_0\,\mathrm{d}V\,, \tag{23}$$

where $V_{\alpha h}$ denotes the section through the space–time element at $t=\alpha h$. $\mathbf{N}_{\alpha h}$ is the matrix of the interpolation functions, determined on the surface $V_{\alpha h}$, $\mathbf{N}(\mathbf{x},\cdot)$ is the matrix of the interpolation functions in the volume $\Omega$, determined in a specified time. The change of the integral limits allows the numerical integration of characteristic matrices. Matrices (20), (21) and (22) have the dimension $N\times 2N$ ($N$ – total number of degrees of freedom). They join moments $t_i$ and $t_{i+1}$.

The more detailed discussion can be found in [15, 21, 22].

### 2.3. Numerical dissipation

Numerical damping of higher frequencies with zero damping of the basic frequency of the structure is an important issue for each time integration method. Several papers on this subject have been published in the open literature (for example [23]). The ideal solution is to control the damping properties of the procedure (in particular cases the damping should be equal to zero). Lower frequencies should not be damped while higher should be damped relatively stronger. With respect to the shape of the damping diagram we can divide all methods in two groups: the first one (Wilson, Houbolt method) with the zero slope of the damping function for small $h/T$, growing with the increase of $h/T$, and the second one (Newmark family methods) with a certain slope of the damping function for $h/T\to 0$. It follows from a practical experience that the first group damps higher modes too much, while the second group does the same with lower modes. Other methods, which use some artificial parameters, improve the damping properties but their use is dangerous since the regular dependence of properties on the parameters does not exist.

Since in the first stage of rolling contact problem the initial penetration (Fig. 11) must be damped rapidly both in high and low frequency ranges, the quality of the damping process is less important than its efficiency. We will also see further on the example that spurious vibration should be controlled and eliminated even in simple testing problems and that it is not easy to damp higher modes in the case of coarse mesh. If we do not so the shape of the time response can be lost. In nonlinear contact problems the question is even more important.

Let us now modify the Eq. (10) by putting

$$\beta=1-\frac{\alpha}{1+\gamma}\,,\quad 0\le\gamma\le 1\,. \tag{24}$$

The resulting system (9), (10) and (24) has the artificial damping which depends on the parameter $\gamma$ and on the moment $\alpha h$ in which the equation of motion is satisfied. Wider investigation of the influence of $\gamma$ on the damping can be found in [24].

## 3. THE SPACE–TIME MODELING OF CONTACT PROBLEM

Dynamic contact problems are characteristic for fast varying contact domains. In some problems the precise definition of the contact zone is of fundamental importance. Contact phenomena with friction that involve vibration of the stick and slip type require both the small time step of the integration of the differential equation of motion and refined mesh in that region. The finite element method gained its popularity since it is relatively simple and universal in applications. However, in certain problems the F.E.M. is difficult since its discrete form does not allow to investigate the problem with the required precision. For example, the varying contact zone, extended between two nodes in spatial mesh requires subintegration of resulting matrices to evaluate more precisely friction contribution. Much more natural approach is to modify the spatial mesh and subintegrate the differential equation in time, in required regions only. Figure 4 shows the classical discrete approach to the problem and the approach with the continuously modified space–time mesh. The

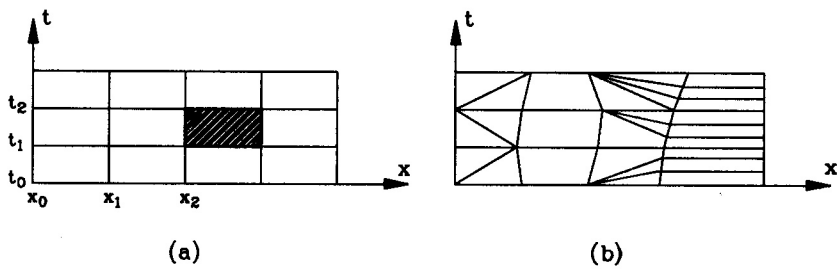


**Fig. 4.** Example of the space-time mesh (a) stationary, (b) non stationary

spatial adaptation of the mesh in structural dynamics can rarely be found in the literature (for example [25, 26, 27]). However, the simplest interpolation of displacement, velocity and acceleration vectors were discussed there with particular reference to additional joint. Such a discontinuous path to the refined/coarsened mesh changes the problem under consideration: local and global stiffness and temporary distribution of acceleration and velocity, compared with the problem solved with the constant mesh. The adaptation procedure may incorporate greater error than the simple classical computation. It is well visible if higher modes are not damped. Although smoothing by physical or numerical damping enhances the quality of the solution, we can not accept such a technique without restrictions.

Subintegration in time carried out in selected areas enables us to describe the contact problem more easily. In Fig. 5 two joints are introduced: $t_c$ – entering of the point into contact and $t_f$ – the end of the contact interval. In practice the whole space–time layer, i.e. all the nodes placed at $t_{i+1}$ and supplementary nodes (sub-division) are treated in the same stage of calculations, in one

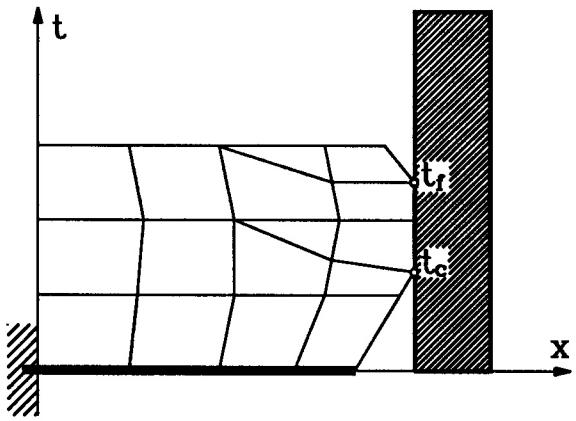


**Fig. 5.** Axial vibration of a bar – space–time mesh in the contact zone

matrix equation. The basics of the space–time finite element method was described in [11, 12, 13, 14]. First the displacement formulation was developed. Then the same idea was extended to derive velocity formulas [15, 21, 22, 24].

### 3.1. Velocity distribution in the contact zone

The velocity of material point entering the contact zone with another body is a discontinuous function (Fig. 6). Two characteristic points of the process are important: entering the contact $t_c$

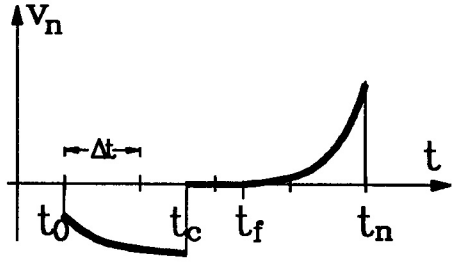


**Fig. 6.** Relative normal velocity in the time interval $[t_0, t_1]$

(this point is a point of discontinuity) and disconnection $t_f$ (this point of discontinuity is less important). In most cases the time interval $\Delta t = t_1 - t_0$ is sufficiently short and it does not contain $t_c$ and $t_f$ in the same time. The discretization should be carried out to determine points $t_c$ and $t_f$ in a natural way. The temporal refinement of the mesh is then required. As a result of the above mentioned discontinuity of the velocity, the geometry (i.e. displacements of joints) can not be determined in a consistent way, i.e. from the velocity field. For example the formula

$$x_1 = x_0 + [(1-\beta)v_0 + \beta v_1]\, h \ , \quad 0 \le \beta \le 1 \tag{25}$$

can not be used. Since $x_1$ is determined by the geometry of bodies and $v_1$ should be equal to zero for $t_c$, then Eq. (25) can be fulfilled approximately only. Two testing examples were performed on the base of the principle depicted in Fig. 5 [21]. They proved the efficiency of the space–time approach.

Now let us discuss the discontinuity of the velocity in contact. This discontinuity shown in Fig. 6 can be removed. At the same time the relation for displacements (7) starts to be consistent. To achieve this point it is necessary to impose the relations derived from the contact conditions to the motion equation in the time step proceeding the detection of the body penetration, i.e. in time $t_0$ if the penetration was detected in $t_1$. The imposed restrictions have to reduce the velocity of the point to such a value $v_0$, for which in the next time step $v_1 = 0$ and $x_1 = x_{\text{cont}}$ (Fig. 7). In the simplest case shown in Fig. 7 the velocity at $t_0$ must have the value

$$v_0 = \frac{x_{\text{cont}} - x_{-1}}{h} - (1-\beta)\, v_{-1}. \tag{26}$$

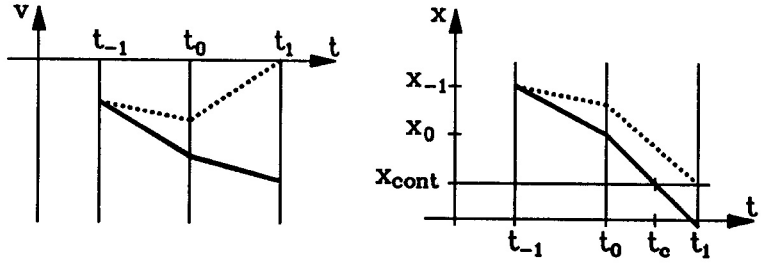


**Fig. 7.** Reduction of the velocity near the contact: continuous line – free motion, dashed line – motion with constraints

The resulting position of the point is

$$x_0 = (1-\beta)x_{-1} + \beta x_{\text{cont}} + (1-\beta)^2 h v_{-1}. \tag{27}$$

At $t = t_1$ the velocity $v_1$ equals 0 and $x_1$ equals $x_{\text{cont}}$.

It should be emphasized that the reduction of the velocity before the contact results in decreasing the energy of the system. It can be implemented in two ways: by imposing the constraint on the velocity of a specified joint or by imposing a predefined breaking force. Both approaches are equivalent since the value of the force is equal to the reaction of contact force in the case of the condition imposed on the velocity of the point. The breaking force acts during the step $\Delta t$. As the effect the node hits an obstacle with the lower velocity and the impact returns less of the momentum after the reflection. The momentum taken off must be given back to the system in the first step in which the point moves freely after the contact.

The following example presents such an approach. The elastic bar with the length $L = 1$, material data $EA = 1$ and $\rho A = 1$, moves with the velocity $v = 1$. In the distance $d = 0.5$ it hits the rigid obstacle. The spatial partition was performed on 8 elements. The parameter $\alpha$ was assumed as 0.8, which gives the unconditionally stable scheme of integration of the time equation.

Figure 8 shows that the velocity after the reflection stays equal to 1. It is even better visible if the observation is carried out during a longer time.

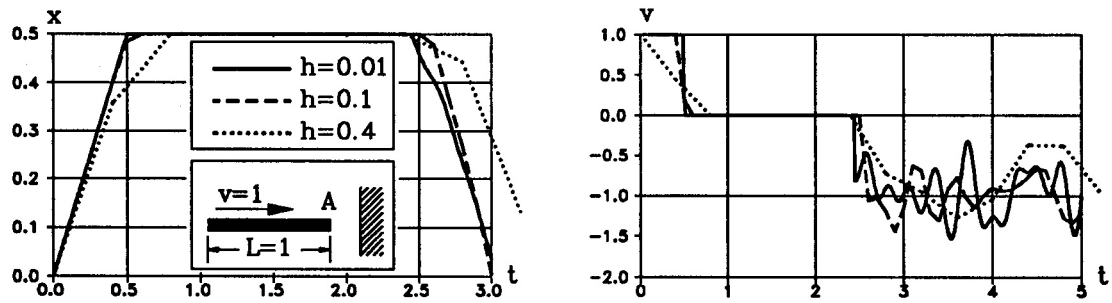


**Fig. 8.** The scheme of the problem and displacements and velocities in time of the heading point A integrated with the time step $h = 0.01$, 0.1 and 0.4

The continuous line is related to the step $h = 0.4$ and shows the point of breaking and return of the momentum. It can also be noticed for $h = 0.1$. The velocity of the bar after the reflection is perturbed by spurious higher order vibration. Small damping improves the response of the system. However, the sufficiently fine spatial discretization is required (Fig. 9).

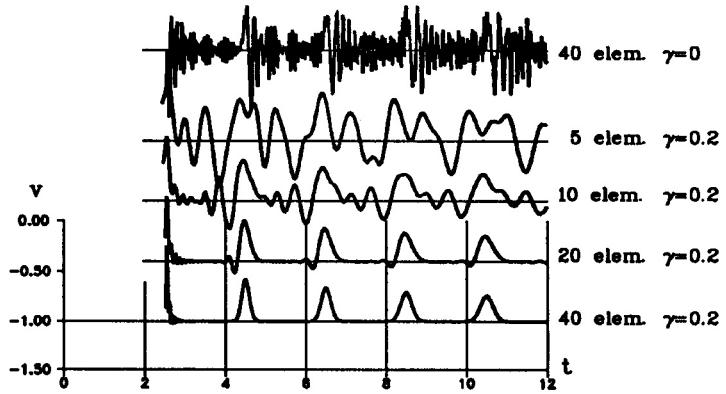


**Fig. 9.** Velocity of the end of the bar after the reflection with different spatial mesh density, without damping ($\gamma = 0$) and with moderate damping ($\gamma = 0.2$) ($\alpha = 0.75$, $h = 0.02$).

In the case of fine partition spurious vibrations have high frequency that should be damped. It can only be achieved if partition into 20 or 40 elements is applied. The partition into 10 spatial elements is insufficient, even in such a simple problem.

The solution algorithm is not complex and can be easily constructed by checking some conditions at every step. Depending on the situation the computation can be continued, the current step must be repeated or we must step back and repeat the previous step. The algorithm is described in Table 1.

**Table 1.** The algorithm of the solution of contact problem with reduction of the speed and momentum restoring.

| | |
|---|---|
| 1° | initially:<br>index=0, step $i$; |
| 2° | block of calculation:<br>$\mathbf{A}\mathbf{v}_{i-1} + \mathbf{B}\mathbf{V}_i + \mathbf{s}_i = \mathbf{F}_i$; |
| 3° | if index=0 and no penetration, then<br>$i := i + 1$, $\longrightarrow$ 2°; |
| 4° | if index=0 and penetration, then<br>given velocity $\bar{v} = (x_{cont} - x_{i-2})/h - (1 - \beta)\, v_{i-2}$,<br>index=1, $i := i - 1$, $\longrightarrow$ 2°; |
| 5° | if index=1, then<br>solve for reactions and hold $\bar{R}$,<br>$\bar{v}$=0, index=2, $\longrightarrow$ 2°; |
| 6° | if index=2 and compression in contact (respective sign of the contact force), then<br>$\bar{v}$=0, $i := i + 1$, $\longrightarrow$ 2°; |
| 7° | if index=2 and tension in contact, then<br>index=0, external force $F$:=$F$+$\bar{R}$, $\longrightarrow$ 2°. |

The method presented was applied in the solution of the contact problem of the deformed wheel running on the rigid base.

## 4. THE ROLLING CONTACT

In the numerical analysis of the rolling contact problem we shall limit the investigation to the range where the contact occurs. Other factors such as friction, plastic deformation, hardening, can simply be added following the classical scheme. As an example we take the wheel with the radius $R$=10 cm, thickness 1 cm, made of steel ($E = 2.05 \cdot 10^7$ N/m$^2$, $\nu = 0.3$, $\rho = 7.83$ g/cm$^3$). It rolls on the rigid base with an angular speed $\omega$. The linear velocities taken into account were of the range 90–180 km/h. The elastic material in plane stress was assumed. The domain was discretized with 864 triangles and 469 nodes (Fig. 10). The uniform mesh density was applied for the reason of wave nature of the process and stress concentration passing throughout the domain.

To avoid multiple rotations of matrices effected by the rotation of the structure and in the same time the accumulation of round-off errors the rotation of the rigid base over the fixed wheel was assumed. All the forces arising from the circular motion were introduced. In the first stage the wheel, which turns is settled slowly on the rigid base (in numerical simulation the base which turns presses slightly the fixed wheel). The depth of penetration (flattening) reaches finally $d = 0.1$ cm (Fig. 11). In order to avoid the influence of the initial conditions and to reduce the effect of wave reflections and interference the comparatively large numerical damping was assumed. The value of the parameter $\gamma$ (24) was equal to 0.2 and it corresponded to the logarithmic decrement of damping $\Lambda = 0.03$. In practice it allowed to damp vibration according to the first eigenform and the period $T \approx 80$ $\mu$s in 95% during the first 1/4 turn of the wheel.

Computation shows that the contact force vary, even when the motion is steady and well damped. First five turns of the wheel with the speed $\omega = 0.3 \cdot 10^{-3}$ rad/s is presented in Fig. 12.

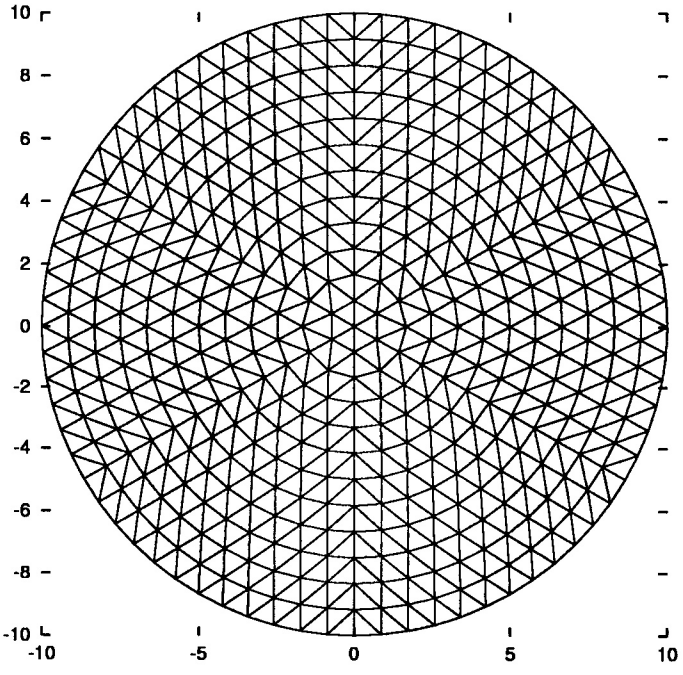


**Fig. 10.** Spatial mesh assumed in calculatin

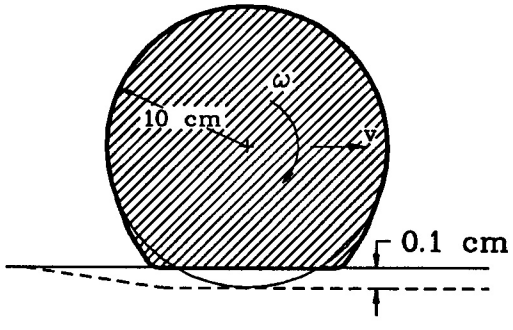


**Fig. 11.** The scheme of the rolling wheel problem

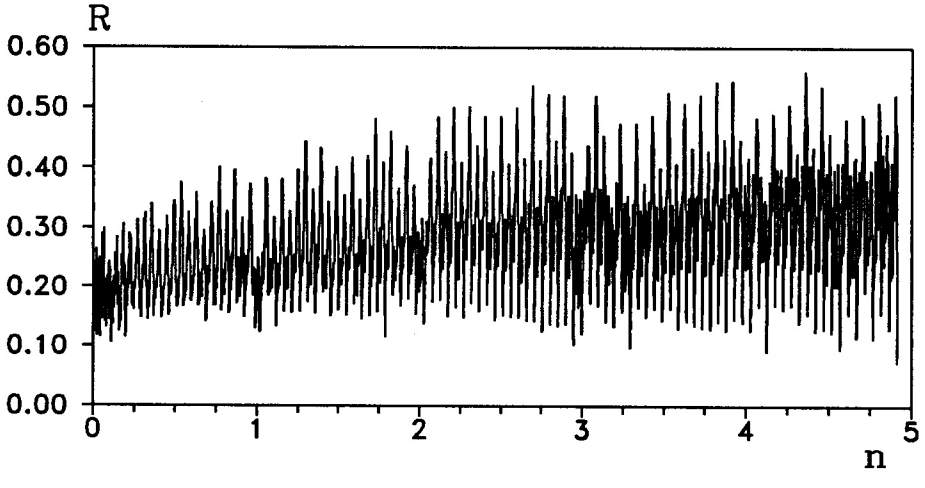


**Fig. 12.** Contact force in successive turns in the case of $\omega = 0.3 \cdot 10^{-3}$ rad/s

The zoom onto the part of the diagram is presented in Fig. 13.

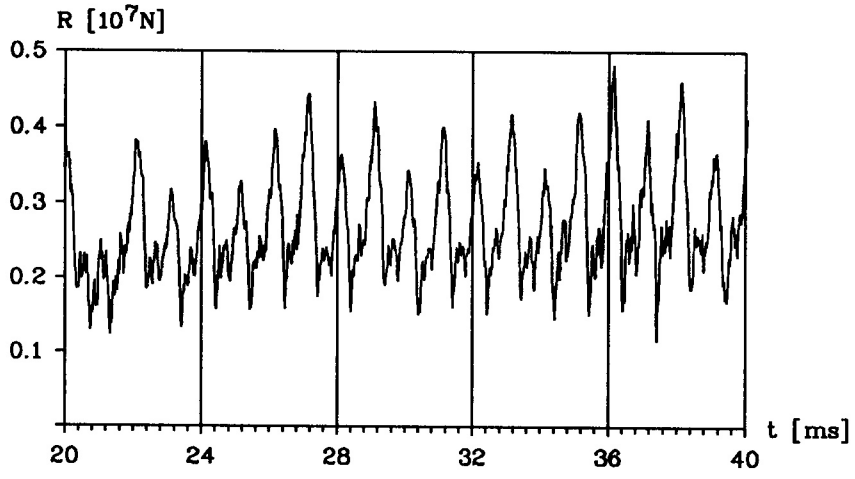


**Fig. 13.** The part of the diagram of the contact force in time

The second invariant of stresses $J_2$ was integrated in successive phases of the full turn. It enables us to show the distribution of stresses in the material (Fig. 14).

It exhibits the periodical distribution of the wear on the wheel surface which can occur during exploitation. The number of contact force oscillations decreases along with the increase of the speed. It was observed for example in [28, 29] for a rubber wheel. However, in those publications the authors treat the problem as an eigenvalue problem. They do not solve the initial boundary problem. The estimated diagram of the relation between the number of oscillations in one full turn and the velocity $\omega$ is shown in Fig. 15.

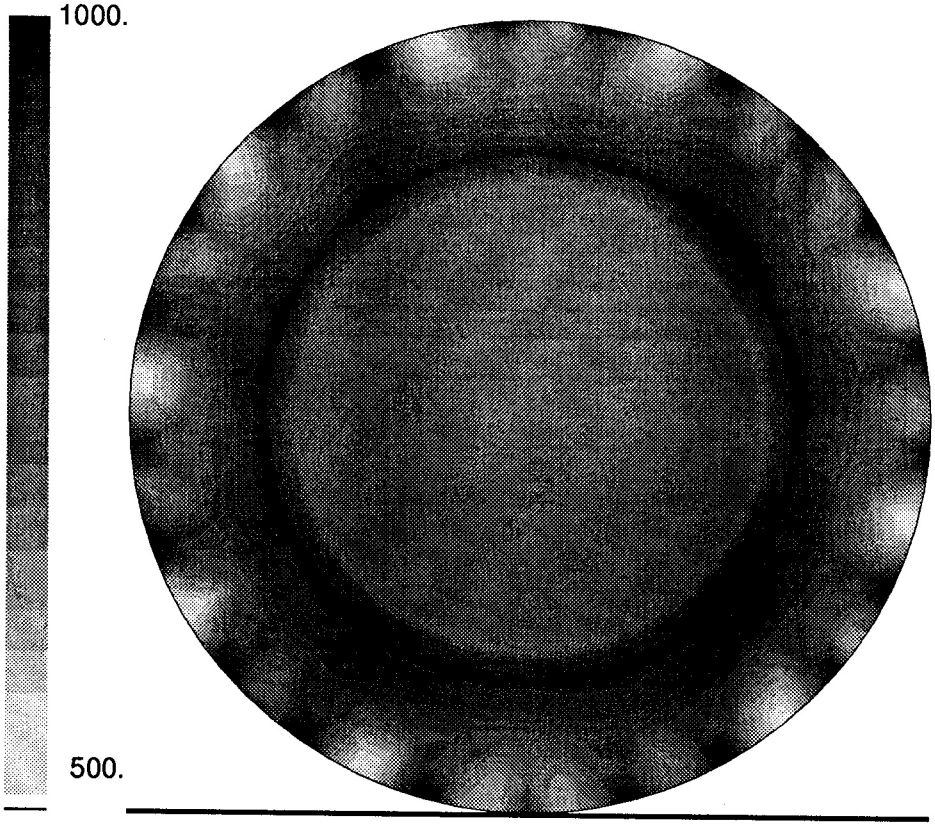


**Fig. 14.** Averaged for the full turn stresses $J_2$ with the velocity $\omega = 0,30 \cdot 10^{-3}$ rad/s [MPa]

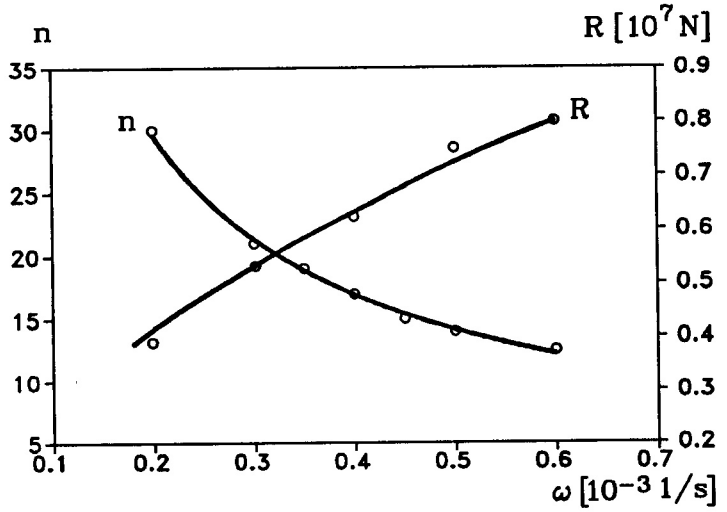


**Fig. 15.** Number of cycles of the reaction and its maximal value in relation of the angular velocity $\omega$

Figure 17 presents the variation of the velocity distribution in successive stages of rolling. The contact zone is located in the lower part of the wheel and moves anti-clockwise (passes from 6 to 5 hour). One can notice that the material vibrates around the wheel axis. Rayleigh waves are observed. The excitation is performed by the contact forces. The value of the contact force increases with the increase of the velocity $\omega$.

For comparison the distribution of $J_2$ performed for higher speed, $\omega = 0.52 \cdot 10^{-3}$ rad/s is presented (Fig. 16). The decrease of the number of waves together with the increase of the strain occurs. In the present solution the plasticity limit is reached in the case of assumed static pressure.

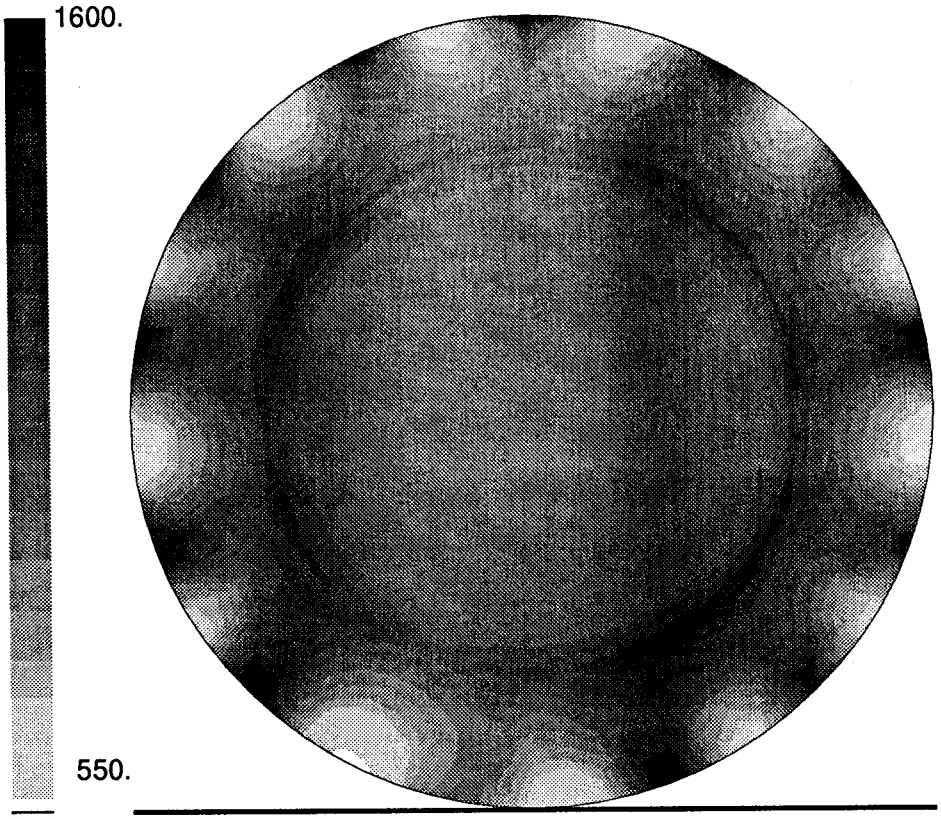


**Fig. 16.** Averaged for the full turn stresses $J_2$ with the velocity $\omega = 0.52 \cdot 10^{-3}$ rad/s [MPa].

The investigation was performed for a full turn of the wheel. If the number of waves due to a turn is not an integer (i.e. the phase shift occurs after each turn), then the diagram is disturbed in the vicinity of the lower point of the wheel, from which the solution starts and on which is finished.

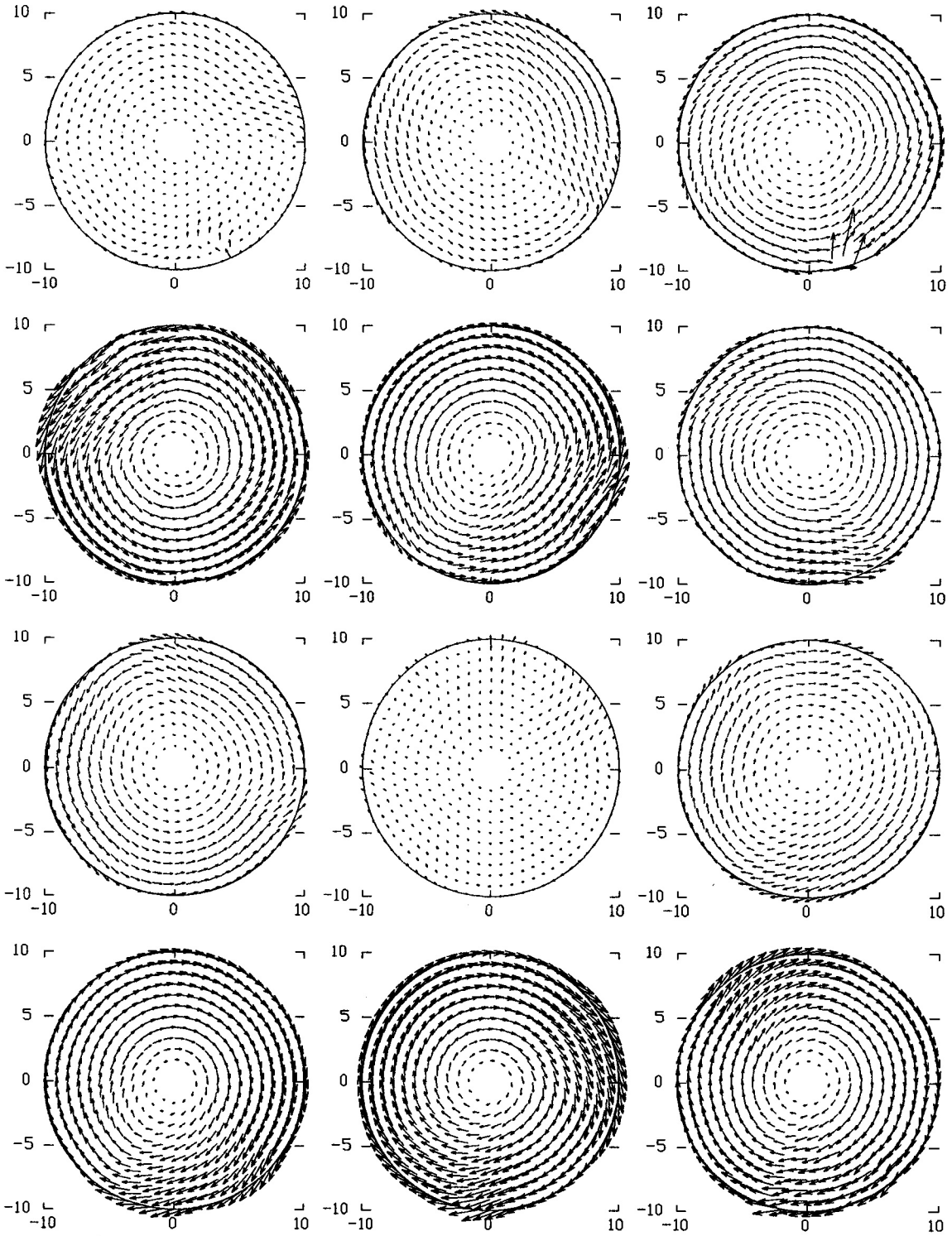


**Fig. 17.** Distribution of velocity in successive stages

## 5. CONCLUSIONS

The efficient method for analysis of dynamic contact problem is presented. The soft way method [15] with modified contact condition described by velocities provides for a convenient treatment of the dynamic contact problem, even in the case of large time steps. The presented method is successfully applied to the problem of corrugations. Even in the simplest case of the material property one can notice the oscillation of the contact force. The resulting stress distribution is stationary if the observation is carried out in the rotating coordinate systems and for the particular value of the angular velocity. If the plastic material was used, the deformation would polygonize the wheel surface permanently. Then successive passages of the wheel over the rail increase the wear by the dynamic feedback [1]. The friction introduced to the contact region can change quantitative relations. It is shown that neither imperfections of rail junctions nor periodic placement of sleepers generate corrugations. Simple stationary motion is disturbed by the propagation of waves from the contact point. In our case the load is introduced kinematically. In the real problem, despite of different type of loading, the situation can be similar due to considerable inertia of the wheelset.

## REFERENCES

[1] K. Knote and K. Hempelmann. The formation of corrugation pattern on the rail tread. A linear theory. In: *2nd Polish-German Workshop on Dynamical Problems in Mechanical Systems*, 77–91, IPPT PAN, Warszawa, 1991.

[2] U. Finberg. Noise generation of railways wheels. In: *2nd Polish-German Workshop on dynamical Problems in Mechanical Systems*, 93–104, IPPT PAN, Warszawa, 1991.

[3] K. Knothe. *Rail Corrugations*. ILR Bericht 56, Berlin, 1983.

[4] B. Ripke and K. Knothe. High frequency wehicle-track interactions in consideration of nonlinear contact mechanics. In: *3rd Polish-German Workshop on dynamical Problems in Mechanical Systems*, 207–218, IPPT PAN, Warszawa, 1993.

[5] O. Mahrenholtz, J. Rońda, R. Bogacz a nd M. Brzozowski. Finite deformation in the rolling contact problem. In: *Proc. Int. Conf. on Nonlinear Mechanics*, 290–295, Shanghai, October 1985.

[6] T. Hirakawa, F. Fujita, m. Kamata and Y. Yamada. Analysis of strip rolling by the finite element method. In: *Advanced Technology of Plasticity*, vol. II, 1132–1137, 1984.

[7] R. Bogacz, J. Rońda and M. Brzozowski. Corrugations in rolling contact problems. *ZAMM*, **67**(11): 567–568, 1987.

[8] R. Bogacz, M. Brzozowski, O. Mahrenholtz and J. Rońda. Dynamic effects in a rolling contact problem. *ZAMM*, **67**(4): T176–T179, 1987.

[9] R.I. Maier. Natural frequency of rail track and its relationship to rail corrugation. In: *Rail Research Papers of B.H.P. Steel International Group*, 89–103, Melbourne, 1976.

[10] R. Bogacz, P. Meinke and S. Dżuła. Vehicle/track-dynamic interaction for high speed frequency range. In: *3rd Polish-German Workshop on dynamical Problems in Mechanical Systems*, 165–179, IPPT PAN, Warszawa, 1993.

[11] C.I. Bajer. Triangular and tetrahedral space–time finite elements in vibration analysis. *Int J. Numer. Meth. Engng.*, **23**: 2031–2048, 1986.

[12] C.I. Bajer. Notes on the stability of non-rectangular space–time finite elements. *Int. J. Numer. Meth. Engng.*, **24**: 1721–1739, 1987.

[13] C.I. Bajer. Adaptive mesh in dynamic problem by the space–time approach. *Comput. and Struct.*, **33**(2): 319–325, 1989.

[14] C.I. Bajer, R. Bogacz and C. Bonthoux. Adaptive space–time elements in the dynamic elastic-viscoplastic problem. *Comput. and Struct.*, **39**: 415–423, 1991.

[15] C.I. Bajer and C. Bohatier. The soft way method and the velocity formulation. *Comput. and Struct.*, **55**(6): 1015–1025, 1995.

[16] C. Bohatier. A large deformation formulation and solution with space-time finite elements. *Arch. Mech.*, **44**: 31–41, 1992.

[17] A. Podhorecki. The viscoelastic space-time element. *Comput. and Struct.*, **23**: 535–544, 1986.

[18] C.I. Bajer and C.G. Bonthoux. State-of-the-art in true space–time finite element method. *Shock Vibr. Dig.*, **20**: 3–11, 1988.

[19] C.I. Bajer and C.G. Bonthoux. State-of-the-art in the space–time element method. *Shock Vibr. Dig.*, **23**(5): 3–9, 1991.

[20] C.I. Bajer and A. Podhorecki. Space–time element method in structural dynamics. *Arch. of Mech.*, **41**: 863–889, 1989.

[21] C. Bohatier and C. I. Bajer. Kinematic approach for dynamic contact problems – the geometrical soft way method. *Engng. Trans.*, **43**(1-2): 101–111, 1995.

[22] C.I. Bajer Space-time finite element formulation for the dynamical evolutionary process. *Appl. Math. and Comp. Sci.*, **3**(2): 251–268, 1993.

[23] H.M. Hilber, T.J.R. Hughes and R.l. Taylor. Improved numerical dissipation for time integration algorithms in structural dynamics. *Earthquake Engng and Struct. Dyn.*, **5**: 283–292, 1977.

[24] C.I. Bajer and R. Bogacz. New formulation of the space-time finite element method for problems of evolution. *Arch. Mech.*, **46**(5): 775–788, 1994.

[25] N.-E. Wiberg, L. Zeng and X. Li. Error estimation and adaptiwity in elastodynamics. *Comput. Meth. Appl. Mech. Engng.*, **101**: 369–395, 1992.

[26] L.F. Zeng and N.-E. Wiberg. Spatial mesh adaptation in semidiscrete finite element analysis of linear elastodynamic problems. *Comp. Mech.*, **9**(5): 315–332, 1992.

[27] L.F. Zeng, N.-E. Wiberg and L. Bernspäng. An adaptative finite element procedure for 2D dynamic transient analysis using direct integration. *Int. J. Numer. Meth. Engng.*, **34**: 997–1014, 1992.

[28] J.T. Oden and T.l. Lin, On the general rolling contact problem for finite deformations of viscoelastic cylinder. *Comput. Meth. Appl. Mech. Engng.*, **57**: 297–367, 1986.

[29] N. Kikuchi and J.T. Oden. *Contact problems in elasticity: a study of variational inequalities and finite element method.* SIAM, 1988.